Journal of Visualization, Vol. 12, No. 2 (2009) 95-107

Regular Paper

Flow Visualization in Arteriovenous Fistula and Aneurysm Using Computational Fluid Dynamics

Bessa, K.L.*[1] and Ortiz, J.P.*[2]

*1 Department of Mechanical Engineering, Polytechnic School, University of São Paulo, 2231 Av. Prof. Mello Moraes, Cidade Universitária, CEP: 05508-900, Brazil.
E-mail: kleiber@usp.br
*2 Department of Mechanical Engineering, Polytechnic School, University of São Paulo, 2231 Av. Prof. Mello Moraes, Cidade Universitária, CEP: 05508-900, Brazil.
E-mail: jportiz@usp.br
Mauá Institute of Technology, Engineering School, S.C. do Sul, e-mail: ortiz@maua.br

Received 31 October 2007
Revised 16 October 2008

Abstract : The arteriovenous fistula (AVF) is characterized by enhanced blood flow and is the most widely used vascular access for chronic haemodialysis (Sivanesan et *al.*, 1998). A large proportion of the AVF late failures are related to local haemodynamics (Sivanesan et *al.*, 1999a). As in AVF, blood flow dynamics plays an important role in growth, rupture, and surgical treatment of aneurysm. Several techniques have been used to study the flow patterns in simplified models of vascular anastomose and aneurysm. In the present investigation, Computational Fluid Dynamics (CFD) is used to analyze the flow patterns in AVF and aneurysm through the velocity waveform obtained from experimental surgeries in dogs (Galego et al., 2000), as well as intra-operative blood flow recordings of patients with radiocephalic AVF (Sivanesan et al., 1999b) and physiological pulses (Aires, 1991), respectively. The flow patterns in AVF for dog and patient surgeries data are qualitatively similar. Perturbation, recirculation and separation zones appeared during cardiac cycle, and these were intensified in the diastole phase for the AVF and aneurysm models. The values of wall shear stress presented in this investigation of AVF and aneurysm models oscillated in the range that can both cause damage to endothelial cells and develop atherosclerosis.

Keywords : arteriovenous fistula, aneurysm, flow visualization, numerical simulation, CFD.

Nomenclature:

AVF	arteriovenous fistula
d_a	artery diameter
d_v	vein diameter
d_{anas}	anastomosis diameter
p	pressure
Re	Reynolds number
t	time
V	velocity
W	Womersley number
w	radian frequency

Greek symbols

∇	gradient operator
δ_s	Stokes layer thickness
μ	dynamic viscosity
ν	kinematic viscosity
ρ	density

1. Introduction

Flow visualization techniques are useful tools for displaying dynamic behavior in liquids and gases. Lee *et al.* (2006) used micro particle image velocimetry technique to investigate high frequency oscillatory ventilation (HFOV) in a micro-channel model of bronchial, and Desse & Tribillon (2006) used a real-time color holographic interferometry (RCHI) to obtain the refractive index itself in two dimensional wake flow. Computational fluid dynamics (CFD) has extended the abilities of engineers and scientists to study flow by creating simulations of the dynamic behavior of fluids under a wide range of conditions. In the present investigation, CFD is used to analyze flow patterns through arteriovenous fistula (AVF) and aneurysm.

AVF is the method of choice for achieving vascular access to chronic haemodialysis in patients with end-stage renal failure, and, is usually performed on the forearm (Fig 1A). The use of AVF over a long period causes the patient to become dependent on the maintenance and functioning of vascular access (Sivanesan et *al.*, 1999b). Quinton, Dillard and Scribner described the first permanent access for chronic haemodialysis in 1960 (Quinton et *al.*, 1960) and the research to find the best way of achieving vascular access still continues. Without an access to a vascular system that can provide an adequate and reliable source of blood flow through the hemodialyzer, haemodialysis becomes impossible. Vascular access should satisfy three criteria: first, it should be suitable for repetitive circulatory access; second, it should allow for a blood flow suitable to conducting high efficiency dialysis, and third, it should minimize treatment complications (Schwab *et al.*, 2001). Some surgical techniques are common in AVF: end-to-side, side-to-side and side-to-side modified (Galego *et al.*, 2000). The flow patterns in AVF can be associated with their possible occlusion. Bassiouny *et al.* (1992) investigated anastomosis intimal thickening related to biomechanical and haemodynamic factors. They showed that there was a complex secondary flow pattern in the vicinity of the suture line. These secondary flow patterns may interact with other biomechanical and humoral factors to modulate suture line intimal thickening. Cole *et al.* (2002) showed that blood flow at the distal junction of the cuffed system is characterized by expansive, low momentum recirculation within the cuff and was also associated with intimal hyperplasia. The visualization of flow patterns is very important for identifying those regions where intimal hyperplasia can develop and how these can be associated with atherosclerosis regions.

An aneurysm is an abnormal widening or ballooning of a portion of the artery, related to weakness in the wall of the blood vessel. Some common locations for aneurysm include: aorta (aortic aneurysm), brain (cerebral aneurysm), leg (popliteal artery aneurysm) and the intestines (mesenteric artery aneurysm). Torii et al. (2001) investigated the effects of blood vessel geometry on haemodynamics of the cerebral artery, especially the internal carotid artery, by using computer graphics, showing that generation and rupture of cerebral aneurysms is strongly correlated with wall shear stress and flow patterns in the blood vessel. Figure 1B shows an aortic aneurysm representation. As in AVF, it is very important to visualize the flow patterns in an aneurysm and associate these with major or minor disturbances in the blood flow. Frydrychowicz *et al.* (2007) visualized local and global vascular haemodynamic in the thoracic aortic. Throughout the visualization, they could compare changes in local blood flow characteristics among both patients in pathological situations and normal volunteers. They could visualize that in pathological situations, there were major disturbances in local blood flow patterns within and even further downstream to the pathology. Asztalos *et al.* (2000) analyzed high shear and stagnation locations which are related to hemolysis and thrombus formation. In such cases, the visualization of flow patterns in the vascular system is very important for understanding the mechanisms involved in pathologies.

The goal of this paper is to visualize the flow patterns in AVF and aneurysm models and to obtain the distribution of wall shear stress (WSS), trying to correlate theses values with pathologies, such as, intimal hyperplasia and atherosclerosis. These pathologies are associated with stagnation, recirculation and separation zones and the high and low values of WSS during the cardiac cycle.

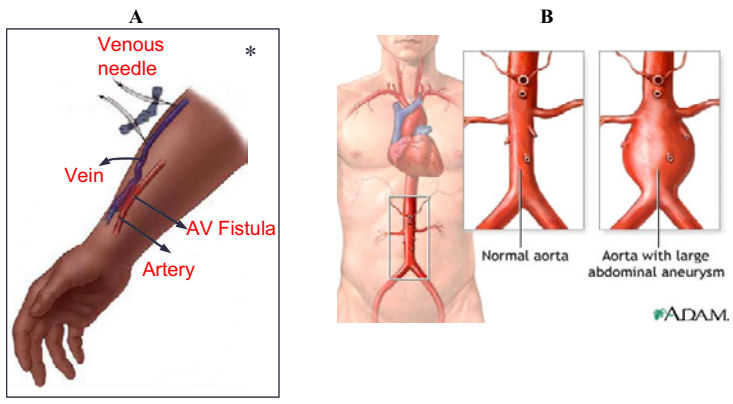

Fig. 1. Schematic representation of an AVF and an aneurysm:
(A) AVF in forearm (Mayo Foundation); (B) normal aorta and aorta with abdominal aneurysm (MedlinePlus).

2. Method

Two geometries were created using software Gambit 2.3.16 (Figs. 2 and 3). The first representing an AVF side-to-side modified model, and, the second, representing an aneurysm model. Choosing the AVF side-to-side modified technique is justified by surgical advantages for haemodialysis patients, according to what was described by Galego (1998).

2.1 Model Geometry - AVF

The recipient artery (d_a) and the vein (d_v) have a diameter of 4 mm and 6mm, respectively (Fig. 2A). The values of the anastomosis diameter (d_{anas}) of 6 mm were obtained according to Galego *et al.* (2000). The anastomosis angle was assumed to be 30°, based on surgical practice. In this work and as a first approach, all vessel walls were assumed to be rigid and the blood flow was considered Newtonian, incompressible and homogenous. Some works, such as that of Hofer *et al.* (1996), showed that when wall distensibility was included in an anastomosis model, the global structures of the flow remained almost the same as when compared to a rigid model, although certain influences of wall distensibility were noted. For example, wall shear stress magnitudes were generally slightly lower in the distensible model, although the mean distribution and magnitudes of wall shear stress were relatively similar in both cases. Two dimensional meshes per AVF model was structured in the artery and unstructured in the vein with a refining mesh in the anastomosis region, coming down to 32,000 active cells (Fig. 2B). The mesh was refined until the flow parameters did not change any further, or rather the results presented in this investigation are mesh independent.

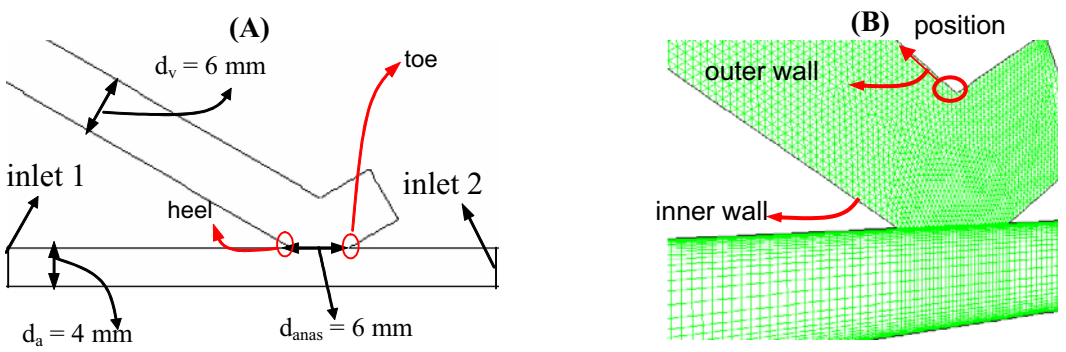

Fig. 2. Schematic representation of an AVF:
(A) side-to-side modified model; (B) hybrid mesh representation.

2.2 Model Geometry - Aneurysm

Aneurysm geometry was developed in three dimensions. The vessel and aneurysm length were 120 mm and 40 mm, respectively. Diameter dilation in the region of the aneurysm was 50%. The diameters of the vessel and aneurysm were 24 and 36 mm, respectively (Fig 3A). As in AVF, the wall vessel was assumed to be rigid and the blood flow Newtonian, incompressible and homogeneous. Three dimensional meshes for the aneurysm model were structured, coming down to 129,630 active cells (Fig. 3B). The mesh was refined until the flow parameters did not change any further, or rather the results presented in this investigation are mesh independent.

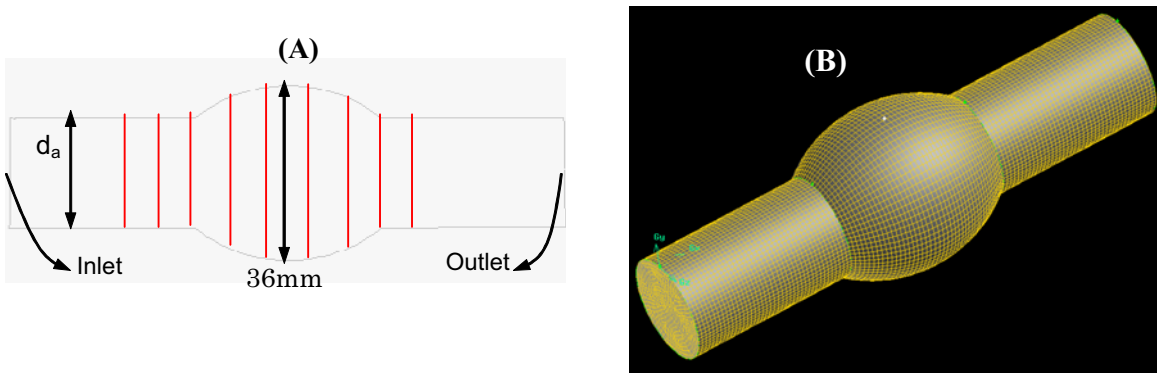

Fig. 3. Schematic representation of an aneurysm:
(A) symmetry plane representation of the aneurysm model (the lines in red represent the transversal sections at which the velocity vectors are plotted); (B) structured mesh representation.

2.3 Numerical Model and Flow Conditions

Mathematic governing equations for incompressible flow and according to the literature (Fox et al., 2006), are presented below:

Mass conservation equation:

$$\nabla.\vec{V} = 0 \tag{1}$$

Momentum conservation equation:

$$\rho\left(\frac{D\vec{V}}{Dt}\right) = -\nabla p + \mu\nabla^2\vec{V} \tag{2}$$

where ρ is the fluid density (kg/m³), $\vec{V}$ is the velocity vector (m/s), t is the time (s), p is the pressure (Pa) and μ is the dynamic fluid viscosity (Pa.s). The CFD code based on the finite volume method (Fluent 6.2.16 Academic License) was used in this study. Discretization of the governing equations at each control volume involved a first order upwind differencing scheme. The resulting system of algebraic equation was solved iteratively using a procedure based on the semi-implicit SIMPLE algorithm. In the AVF and aneurysm models, the inlet velocity profiles were maintained uniform across the inlet cross section. The outlet condition requires that velocity gradients in flow direction be zero. This condition is acceptable due to the outlet boundary having been located far downstream from the junction, in the case of AVF, or far from the arterial enlargement, in the case of the aneurysm. The no slip condition was applied to all the walls.

Fluid properties were assumed according to the literature (Berger et al., 1996): ρ = 1050 kg/m³ and μ = 3.45 mPa.s.

The simulation of AVF was performed by using mean velocity data obtained from experimental surgery on dogs through an electromagnetic flow meter (Galego et al., 2000), where mean velocity was measured at the proximal artery, distal artery and vein (Fig. 4).

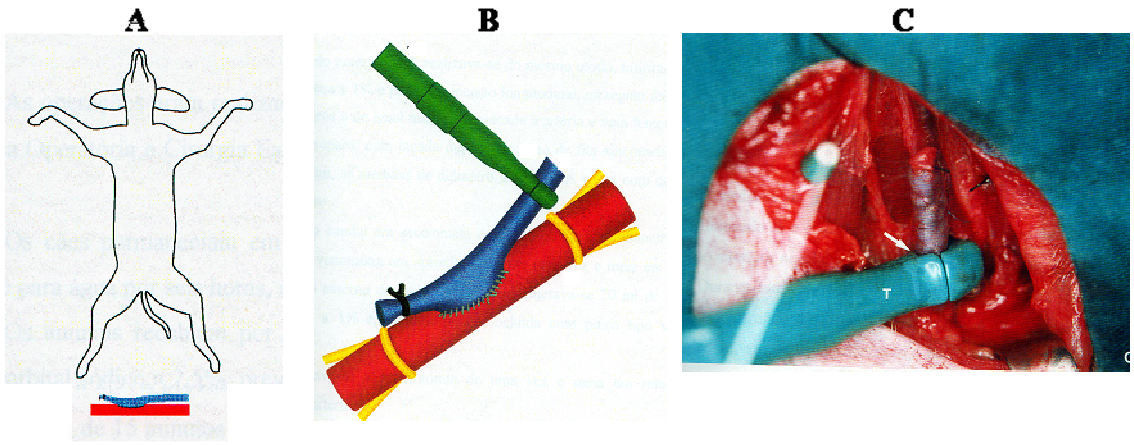

Fig. 4. Schematic representation in dog experimental surgery:
(A) dog position in experimental surgery; (B) side-to-side modified AVF with electromagnetic flowmeter representation; (C) flow measurement with electromagnetic flowmeter in the experimental surgery (Galego et al., 2000).

Sine wave functions were adjusted and inserted at inlet boundaries 1 and 2 (Fig. 2A), based on experimental dog surgery data (Fig. 5). The simulation of AVF was also performed from intraoperative blood flow recordings of patients with radiocephalic AVF (Sivanesan et al., 1999b). The waveform, in this case, is shown in the figure 6. The yellow squares in figures 5 and 6 indicate the instant time at which the simulated velocity profile was plotted. Each pulse cycle was divided into 100 time steps of 7.56 ms and 1 ms, respectively.

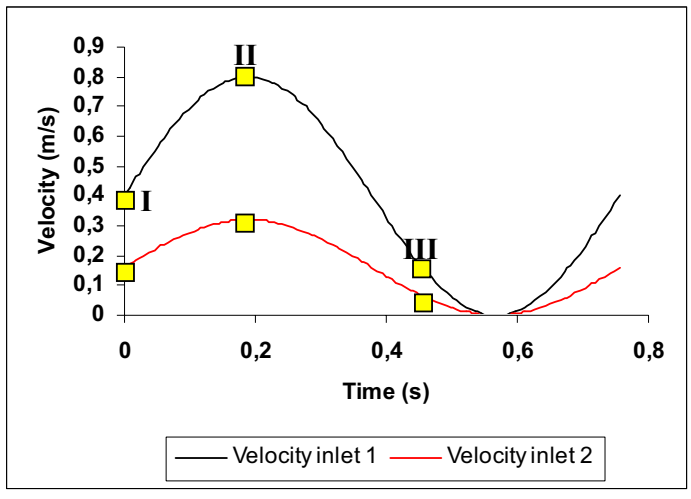

Fig. 5. Velocity sine waveform adjusted to AVF model from dog experimental surgeries.

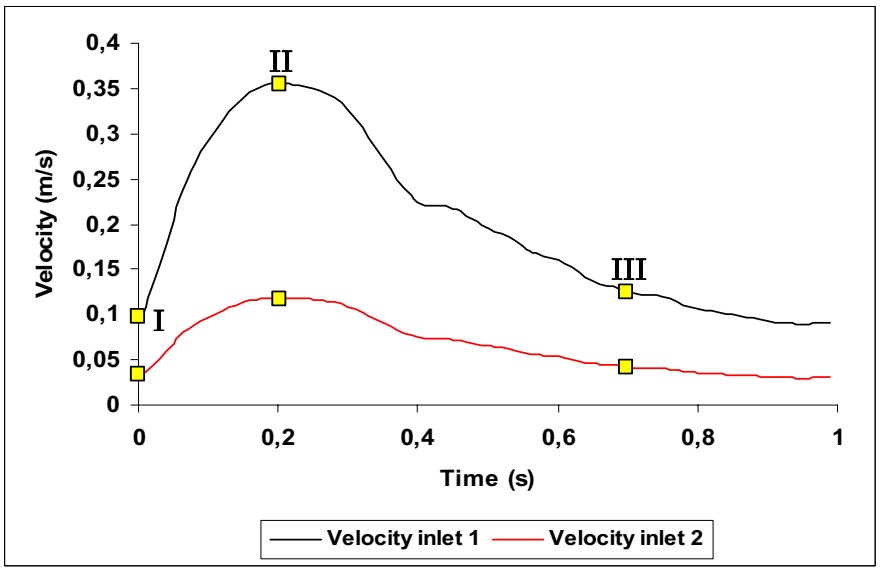

Fig. 6. Velocity waveform obtained from intraoperative recordings of patients.

Flow simulation in the aneurysm was performed by using velocity waveform data from physiological pulses (Aires, 1991) (Fig. 7). The velocity waveform was inserted at the inlet boundary (Fig. 3A). The yellow squares in figure 7 indicate the instant time at which the velocity profile was plotted. Each pulse cycle was divided into 100 time steps of 9 ms size.

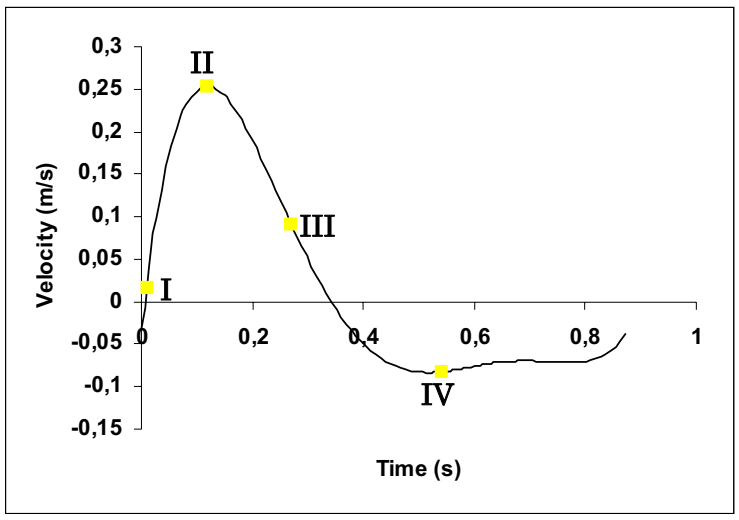

Fig. 7. Velocity waveform obtained from physiological pulses (Aires, 1991).

Reynolds numbers, which are defined by the inertia and the viscous force, were calculated based on mean and peak velocities values (Figs. 5, 6 and 7):

$$\mathrm{Re} = \frac{V d_a}{\nu} \tag{3}$$

where, V is the mean or peak velocity in the artery (m/s), d_a is the artery diameter (m) and ν is the kinematic viscosity (m^2/s).

In a pulsatile flow, the pulse rate is determined by the Womersley number (W), which relates the frequency of a pulsatile wave and the viscous force:

$$W = \frac{d_a}{2}\sqrt{\frac{w}{v}} \tag{4}$$

where, w is the radian frequency. According to the concept of the Stokes layer, the parameter δ_s of Stokes layer thickness or viscous wave penetration depth was calculated based on the equation (5):

$$\delta_s = 5\sqrt{\frac{v}{w}} \tag{5}$$

3. Results

Figure 8 shows the velocity contours behaviour in the AFV model at various instants in time chosen during the cycle for experimental dog and patient surgeries (Figs. 5 and 6). Values attributed to velocity in the model based on experimental dog surgery data, are higher than those from patient surgery data. During the instant time I, although flow separation occurs as a function of AVF geometry, the flow pattern is almost straight. In the instant time II, which corresponds to velocity peak, wavy flow, recirculation and separation zones are observed. These recirculation and separation zones are intensified during flow deceleration (instant time III – diastole phase), mainly in experimental dog surgery data.

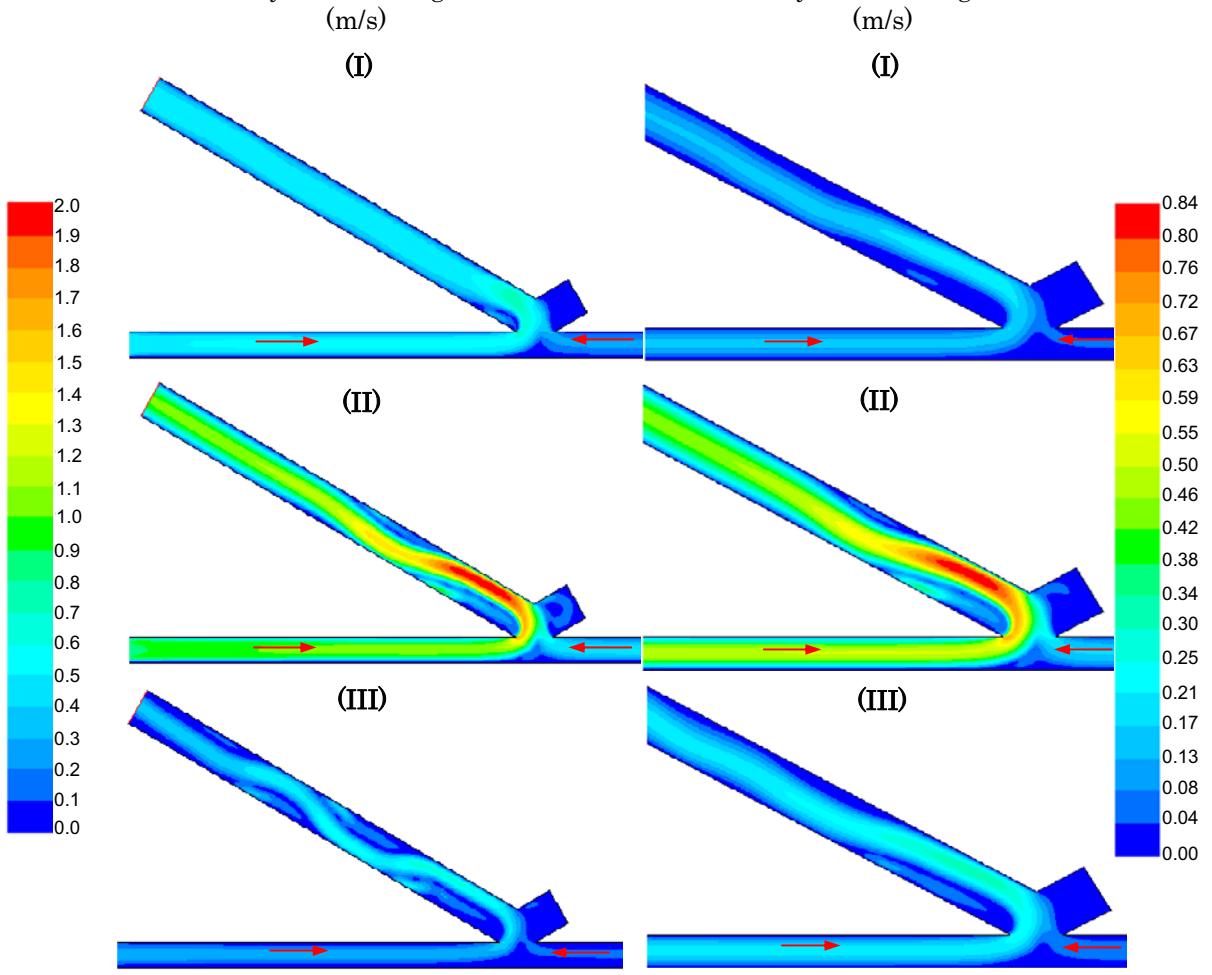

Fig. 8. Velocity contour magnitude in AVF model at various instants time during the waveform cycle.

Figure 9 shows velocity vectors behaviour in the AVF model for several instants time chosen during the cycle (Figs. 5 and 6) for experimental dog and patient surgery data. The results showed in the figure 8 and in the figure 9 are similar, however, in the figure 9, the velocity profile can be seen in all AFV model through vectors velocity. Therefore, recirculation and separation zones are better visualized. In the instant time I, flow patterns are almost straight with a recirculation zone in the vein, near the heel, for experimental dog surgery data, but with a larger recirculation zone in the vein for patient surgery data. As the fluid from the proximal artery (left) enters the anastomosis, it separates at the heel (inner wall) where a vortex with anticlockwise rotation is formed. Stagnation points can be seen on the floor of the artery and on the inner wall close to the heel. In the instant time II, recirculation and separation zones are increased downstream in the vein, and flow patterns show a vortex with a clockwise rotation in the outer wall beside the vortex with anticlockwise rotation next to the heel. These recirculation and separation zones become intensified during flow deceleration, according to fig. 9 (instant time III).

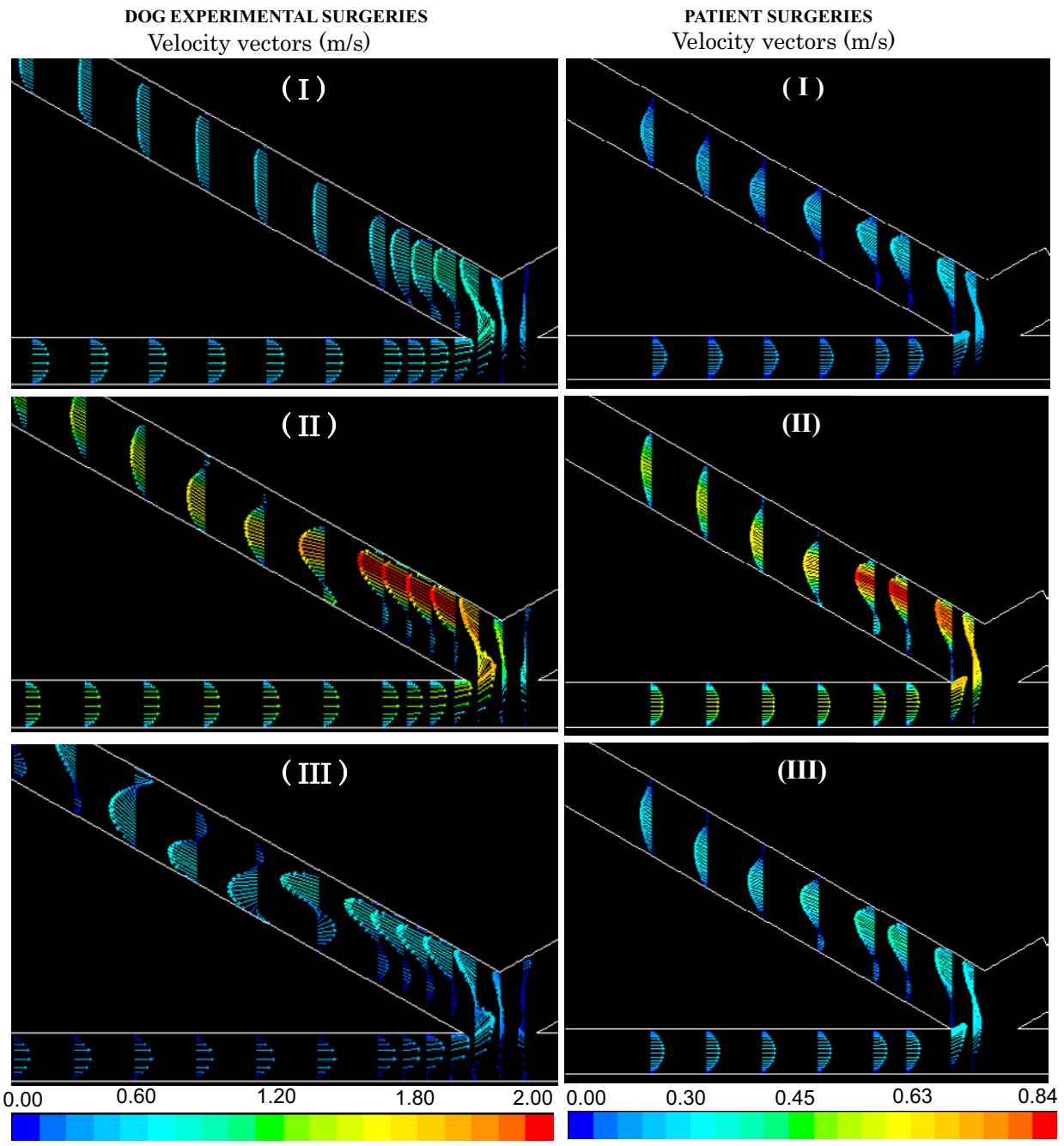

Fig. 9. Velocity vectors in AVF models.

Figure 10 shows velocity vectors and streamlines behaviour in the aneurysm model at several instants time during the cycle (Fig. 7). The vortex formation is better visualized in the streamlines. In the beginning of the cycle (instant time I), flow patterns were straight. Instant in time II presents the highest velocity values of the cycle and flow patterns were still straight. In the instant time III, the velocity profile becomes inverted inside the aneurysm, with the formation of a vortex at the bottom and the top of the aneurysm. In the instant time IV, the velocity profile has been completely inverted and the vortex pair, which appeared in the instant time III, has shifted towards the center of the aneurysm.

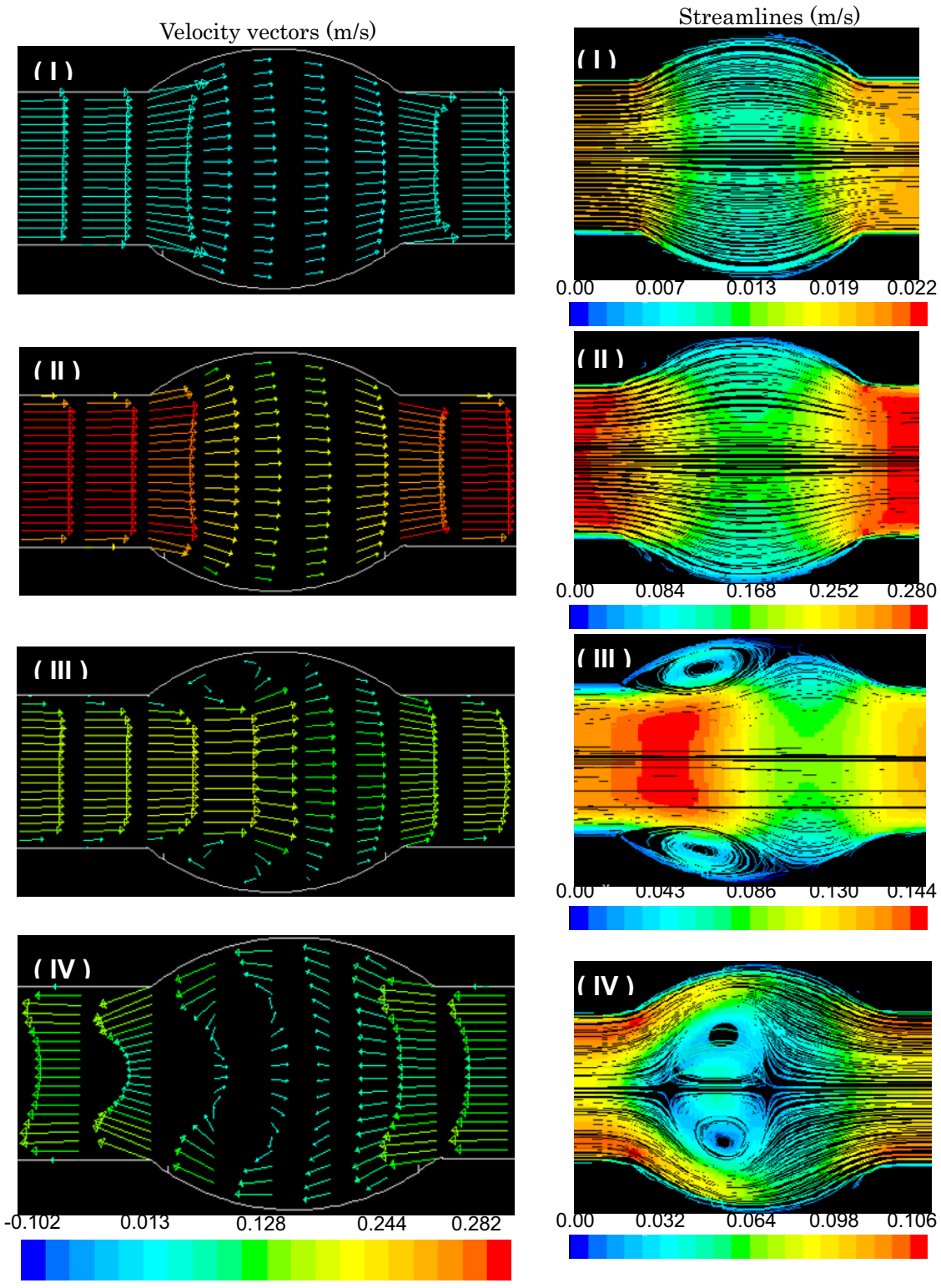

Fig. 10. Velocity vectors and streamlines at various instant time of the cycle for aneurysm model.

Figure 11 shows wall shear stress distribution in the outer wall of AVF (Fig. 2) and in the aneurysm in the instant time II (for velocity peak). For the AVF model, wall shear stress values oscillated between -60 and 20 Pa for experimental dog surgery data and –17 and 4 Pa for patient surgery data. For the aneurysm model, these values oscillated between 0 and 3 Pa.

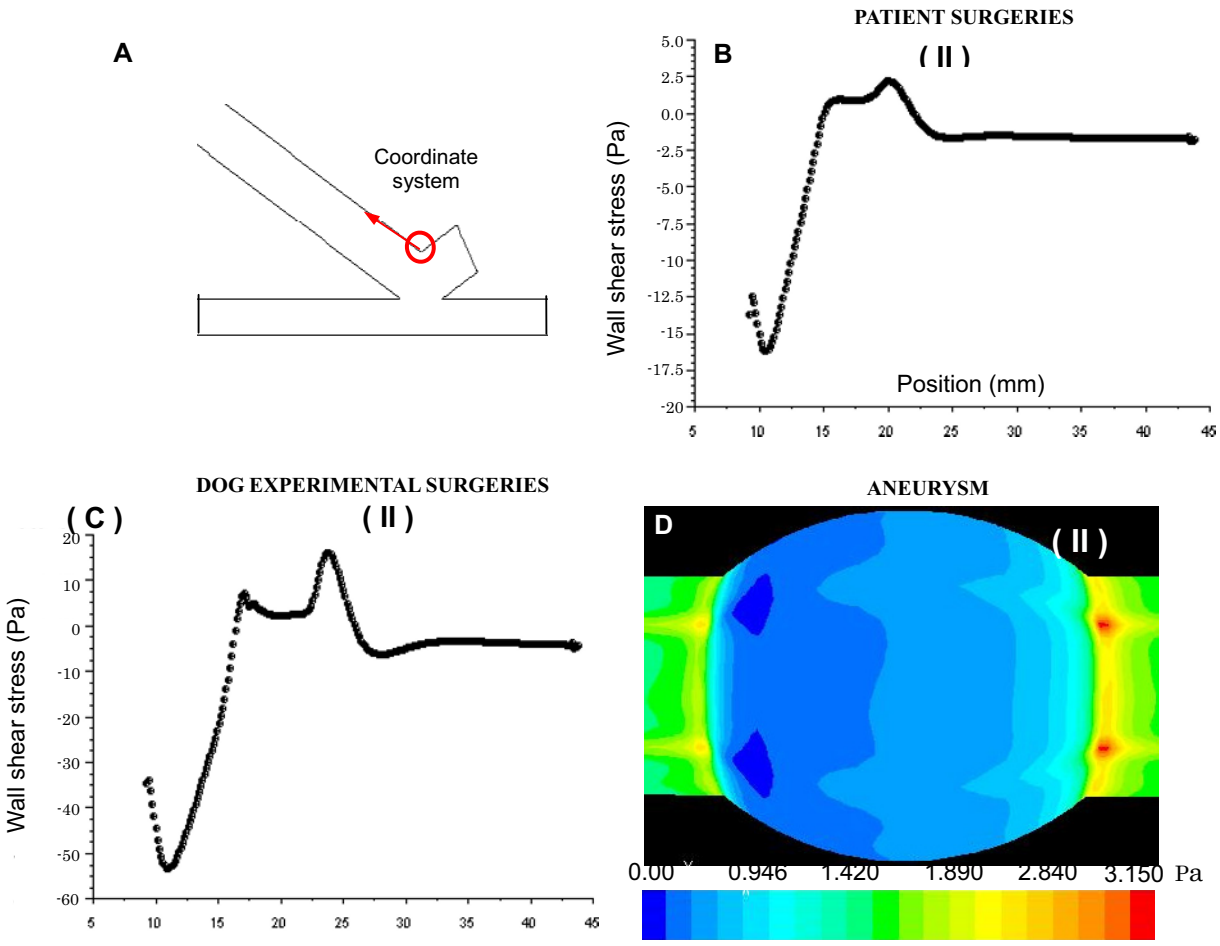

Fig. 11. Shear stress distribution in the outer wall of the AVF and in the aneurysm models: (A) coordinate system in the outer wall of the AVF; (B and C) shear stress values (Pa) obtained from numerical simulations in patients surgeries and in dog experimental surgeries, respectively; (D) shear stress values (Pa) in aneurysm.

The calculated values of Reynolds numbers (mean and peak), of Womersley number and of viscous wave penetration depth are shown in table 1, for the artery vessel:

Table 1. Values of Reynolds and Womersley numbers and viscous wave penetration depth.

	Re_{mean}	Re_{peak}	W	δ_s (mm)	d_a (mm)
AVF Dog	467	915	2.8	3.2	4
AVF Patient	230	411	2.7	3.7	4
Aneurysm	960	1715	17	3.5	24

These parameters interpretation are very important for understanding how they influence the velocity profile. Poiseuille parabolic velocity is obtained when there is a constant pressure gradient. However, the velocity profile is altered when there is an oscillatory pressure gradient. If the pressure gradient variation is slow, it is reasonable to expect that the velocity profile at each instant of time has a parabolic distribution whose maximum amplitude is directly proportional to the instantaneous

value of the pressure gradient. This situation corresponds to a quasi-steady flow. When pressure gradient oscillation frequency rapidly increases (high Womersley numbers), the velocity profile will not be able to respond immediately to the changing pressure gradient, thus the effects of unsteadiness become manifest. For the velocity profile to faithfully follow the varying time pressure gradient, it would be necessary for the viscous penetration depth to be, at least, equal to the tube radius.

4. Discussion and Conclusions

In this work, the flow visualization in AVF and aneurysm models was obtained through numerical simulation using Fluent 6.2.16. For models studies, geometries of the AVF and aneurysm were simplified: the vessels segments were uniformly circular, the artery was straight, the anastomosis was planar, i.e. the vein and the artery were on the same plane and compliance was not reproducible. However, this model (AVF) incorporated a similar vein to the artery diameter ratio as seen *in vivo* (Galego *et al.*, 2000).

According to what was shown before, visualization of the flow patterns is very important to understand how certain haemodynamic parameters can be involved in the development of pathologies. From the literature, stagnation and recirculation zones are propitious regions for developing atherosclerosis. Atherosclerosis is associated with excessive near wall residence times and deposition of blood particles, such as platelets and monocytes, and is also associated with intimal hyperplasia development (Sottiurai, 1999). During the cardiac cycle, 1/3 of the time is attributed to the systolic phase and 2/3 to the diastolic phase. According to the results presented here, perturbation, recirculation and separation zones appear and are intensified during the diastolic phase (AVF - Figs. 8 and 9; aneurysm – Fig. 10) and contribute to the excessive near wall residence time. The recirculation and separation zones are more pronounced for experimental dog surgery data when compared with patient surgery data. Although these data were taken from different surgical conditions for femoral AVF experimental dog surgeries and for radiocephalic AVF patients surgeries, respectively, and although the range of velocities and shear stress are different, the flow standard is about the same, when these two cases are compared. Inside the aneurysm, the vortex pair appears with the complete inversion of velocity profile. All these alterations in the flow patterns during the diastolic phase can cause damage in endothelial cells, thus contributing to promote endothelial dysfunction.

Fry (1968) had reported that the values of wall shear stress between 35 and 40 Pa can cause physical damage in endothelial cells within an hour of exposure. Lower values of wall shear stress (10 to 30 Pa) can increase the permeability of the endothelial cells, damaging erythrocytes (Blackshear, 1972) and causing enhanced platelet adhesiveness and platelet aggregation (Malek *et al.*, 1999). Lower values of wall shear stress, below 1 Pa, have shown to be associated with the development of intimal hyperplasia in arterial anastomosis (Sallam *et al.*, 1996), and in the development of atherosclerosis (Malek *et al.*, 1999). The values of wall shear stress presented in figure 11 oscillated over a range that can both cause damage in endothelial cells and develop atherosclerosis. Further research is, however, necessary to quantify this range of values, so that modeling calibration promotion, based on experimental surgeries, could be possible.

Berger *et al.* (1996) showed typical values of the Womersley number (W) in aorta and femoral arteries of several animals. For the femoral artery of dogs and the aorta artery of humans, the Womersley numbers are 2.4 and 15, respectively, which are near to the results presented in table 1, 2.8 and 17. The velocity profile obtained in the artery of the AVF is parabolic during all the cardiac cycle, and, this fact occurs due to the Womersley number being small and viscous wave penetration depth higher than the tube radius. The wavy flow in the vein (AVF) occurs due to a change in the flow direction and to flow separation in the anastomosis. In the aneurysm model, the velocity profile is practically flat due to the higher Womersley number (W = 17) and the smaller viscous wave penetration depth (smaller than the tube radius). Therefore, the fluid near the wall of the tube,

which has a lower velocity than that near the axis, responds more rapidly than the core fluid to the changing pressure gradient, this meaning that there is a tendency for a uniform velocity profile (Fig. 10). The Reynolds number is also an important dimensionless parameter and the values obtained in the artery are under 2000, according to table 1, which means that the flow was considered laminar. Further research is, however, necessary to reach the critical Reynolds number for pulsatile flow.

Summarizing, the flow patterns in AVF for dog and patient surgery data are qualitatively similar, even though they are quantitatively different, when considering different flow boundary conditions. The flow patterns in both models, AVF and aneurysm, are complex and recirculation and separation zones occurring in these flows are mainly associated to the diastole phase of the cycle, contributing to the development of pathologies, such as, intimal hyperplasia and atherosclerosis.

Acknowledgements

The first author would like to thank the financial support of graduate scholarship from Conselho Nacional de Desenvolvimento Científico e Tecnológico (CNPq) (Brasília, Brazil). The authors would also like to acknowledge Institute Dante Pazzanese de Cardiologia – IDPC/SP through Eng. Daniel F. Legendre.

References

Aires, M.M. (1991), "Fisiologia (Physiology)", Rio de Janeiro: Guanabara Koogan S.A. (in Portuguese).
Asztalos, B., Yamane, T., Nishida, M., Masuzawa, T., Konishi, Y. (2000), "Evaluation of shear and recirculation in centrifugal heart by flow visualization", Journal of Visualization 1, 79-92.
Bassiouny, H.S., S. White, S. Glagov, E. Choi, D.P. Giddens, C.K. Zarins (1992), "Anastomotic intimal hyperplasia: Mechanical injury or flow induced", J Vasc Surg, 15, 708-717.
Berger, S.A., W. Goldsmith, E.R. Lewis (1996), "Introduction to Bioengineering", England: Oxford University Press.
Blackshear, P.L. (1972), "Mechanical hemolisys in flowing blood", In: Fung, Y.C., Perrone, N., Anliker, M. (eds.), Biomechanics: Its Foundation and Objectives. Prentice-Hall, Englewood Cliffs, 501-528.
Cole, J.S., J.K. Watterson, M.J.G. O'Reilly (2002), "Is there a haemodynamic advantage associated with cuffed arterial anastomoses?", Journal of Biomechanics, 35, 1337-1346.
Desse, J.M. & Tribillon, J.L. (2006), "State of the Art of Color Interferometry at ONERA", Journal of Visualization 9, 363-372.
Fox, R.W., McDonald, A.T., Pritchard, P.J. (2006), "Introdução à mecânica dos fluidos". LTC editora, tradução para o português sexta edição, 798 p.
Fry, D.L. (1968), "Acute vascular endothelial changes associated with increased blood velocity gradients", Circulation Research, 22, 165-197.
Frydrychowicz, A., A. Harloff, B. Jung, M. Zaitsev, E. Weigang, T.A. Bley, M. Langer, J. Hennig, M. Markl (2007), "Time-resolved, 3-dimensional magnetic resonance flow analysis at 3 T: visualization of normal and pathological aortic vascular hemodynamics", Journal of computer assisted tomography, 31, 9-15.
Galego, S. J. (1998), "Estudo comparativo do fluxo nas fístulas arteriovenosas femorais, término-lateral e látero-lateral modificada de cães", Dissertação apresentada a Universidade Federal de São Paulo – UNIFESP, 80 p.
Galego, S.J., S. Goldenberg, J.P. Ortiz, P. Deoliveira Gomes, E. Ramacciotti (2000), "Comparative blood flow of arteriovenous fistulae in canine femoral arteries: modified latero-lateral and end-lateral techniques", Artificial Organs, 24, 235-240.
Hofer, M., G. Rappistsch, K. Perktold, W. Trubel, H. Schima (1996), "Numerical study of wall mechanics and fluid dynamics in end-to-side anastomoses and correlation to intimal hyperplasia", Journal of Biomechanics, 29, 1297-1308.
Lee, W.J., Kawahashi, M., Hirahara, H., (2006), "Experimental Investigation of Oscillatory Air Flow in a Bronchial Tube Model with HFOV Mode", Journal of Visualization 9, 39-48.
Malek, A.M., S.L. Alper, S. Izumo (1999), "Hemodynamic shear stress and its role in atherosclerosis", JAMA, 282, 2035-2042
Mayo Foundation for Medical Education and Research - http://www.mayo.edu/.
MedlinePlus Health Information from the National Library of Medicine - http://www.nlm.nih.gov/medlineplus/
Quinton, W.E., D. Dillard, B.H. Scribner (1960), "Cannulation of blood vessels for prolonged haemodialysis", Trans Am Soc Artif Intern Organs, 6, 104-113.
Sallam, T.A., A.B. Lumsden, W.D. Suggs, D.N. Ku (1996), "Low shear stress promotes intimal hyperplasia thickening", Journal of Vascular Investment, 2, 12-22.
Schwab, S.J., M.J. Oliver, P. Suhocki, R. McCann (2001), "Hemodialysis arteriovenous access: Detection of stenosis and response to treatment by vascular access blood flow", Kidney International, 59, 358-362.
Sivanesan, S., T.V. How, A. Bakran (1998), "Characterizing flow distributions in AV fistulae for haemodialysis access", Nephrology Dialysis Transplatation, 13, 3108-3110.
Sivanesan, S., T.V. How, A. Bakran (1999a), "Sites of stenosis in AV fistulae for haemodialysis acess", Nephrology Dialysis Transplantation, 14, 118-120.
Sivanesan, S., T.V. How, R.A. Black, A. Bakran (1999b), "Flow patterns in the radiocephalic arteriovenous fistula: an in vitro study", Journal of Biomechanics, 32, 915-925.
Sottiurai, V.S. (1999), "Distal anastomotic intimal hyperplasia: histocytomorphology, pathophysiology, etiology, and prevention", Int. J. Angiol., 8, 1-10.
Torii, R., Oshima, M., Kobayashi, T., Takagi, K (2001), "The hemodynamic study of the cerebral artery using numerical simulations based on medical imaging data", Journal of Visualization 3, 277-284.

Author Profile

Jayme Ortiz: He received his BE degree in Civil Engineering from Mackenzie University – São Paulo, in 1972. In 1977/1978 took up a "Perfezionamento" course from Padova University/Istituto di Idraulica di Padova. He received his Master's degree (Eng) from the University of SãoPaulo/Polytehcnic School in 1982. He took up a "Sandwiche" Doctorate Course in the University of São Paulo/University of Minnesota getting his Doctor degree (Eng) from the University of São Paulo/Polytechnic School in 1989. He was an Honorary Fellow of Saint Anthony Falls Hydraulic Laboratory/University of Minnesota between 1987 and 1989. Currently, he is a Professor of the University of São Paulo/Polytechnic School and of the Mauá Institute of Technology/Engineering School. His main areas of research and consulting are in Fluid Mechanics and Hydraulics, with a special emphasis on numerical and physical modeling applied to Hydraulic Structures, Biomedical Engineering and Ocean and Fluvial Wastewater Disposal. He is a member of IAHR, MWWD, ABRH and ABCM.

Kleiber Bessa: He received his BE degree in Mechanical Engineering from Federal University of Rio Grande do Norte – in 2000 and Master degree (Eng.) in Mechanical Engineering in 2004 from University of São Paulo. He concluded his DE in Mechanical Engineering in 2008 at the same University. He has worked with numerical and physical simulation in the following areas: Fluid Mechanics applied to Biomedical Engineering and Ocean and Fluvial Wastewater Disposal.